

Three-dimensional finite element modeling of a long-span cable-stayed bridge for local stress analysis

Chartree Lertsima[†] and Taweep Chaisomphob[‡]

*Civil Engineering Program, Sirindhorn International Institute of Technology, Thammasat University,
Pathumthani 12121, Thailand*

Eiki Yamaguchi[‡]

Department of Civil Engineering, Kyushu Institute of Technology, Tobata, Kitakyushu 804-8550, Japan

(Received October 21, 2003, Accepted February 16, 2004)

Abstract. The information on local stress acting in a bridge is required in many occasions such as fatigue assessment. The analysis by beam elements cannot yield this class of information adequately, while the finite element modeling of an entire long-span bridge by shell elements is impractical. In the present study, the hybrid modeling is tried out: only part of a bridge in which the point of interest is located is discretized by shell elements and the remaining part is modeled by beam elements. By solving a simple box girder problem, the effectiveness of this approach is discussed. This technique is then applied to the Rama IX Bridge for local stress evaluation. The numerical results compare very well with the results of a full-scale static loading test. The present research thus offers a practical yet accurate technique for the stress analysis of a long-span cable-stayed bridge.

Key words: three-dimensional finite element modeling; cable-stayed bridge; hybrid modeling; local stress analysis; full-scale static loading test.

1. Introduction

The finite element analysis (FEA) of a cable-supported bridge is often carried out in two dimensions (2D) to capture its basic structural characteristics (Karoumi 1999, Kim and Lee 2001, Wang *et al.* 2002, Au *et al.* 2001, Agrawal 1997, Wang and Yang 1996). The behavior of a cable-supported bridge however can be complicated since it is statically indeterminate and exposed to dynamic and static loads. Therefore, FEA in three dimensions (3D) is needed for a thorough insight into the realistic structural behavior of a bridge. In most of this class of analysis, beam and truss elements are employed and various aspects of a bridge are investigated (Ali and Abdel-Ghaffar 1995, Zhang *et al.* 2001, Shu and Wang 2001, Xu *et al.* 1997, Chang *et al.* 2001). The enhancement of these elements is also challenged (Karoumi 1999, Kim and Lee 2001, Ali and Abdel-Ghaffar 1995).

[†] Ph. D. Student

[‡] Associate Professor

The information on local stress in a bridge is required in many occasions such as fatigue assessment. The analysis by beam and truss elements cannot yield this class of information adequately, while the modeling by beam and truss elements is sufficient and effective for analyzing the global behavior of a bridge. On the other hand, the finite element modeling of an entire long-span bridge by more sophisticated 3D elements such as shell elements is not practical even at the current stage of development of computer technology, although such an effort has been initiated (Ali and Abdel-Ghaffar 1995, Chang *et al.* 2001, Karoumi 1999, Kim and Lee 2001, Shu and Wang 2001, Wang *et al.* 2002, Zhang *et al.* 2001, Xu *et al.* 1997).

In the present study, the local stress of a long-span cable-stayed bridge, in particular the Rama IX Bridge in Bangkok, Thailand, is evaluated. Since the modeling of this whole bridge by shell elements is impractical, the hybrid finite element modeling is tried out. In this approach, the portion of the bridge that contains the point for local stress evaluation is modeled by shell elements whereas the rest is modeled by beam elements. By solving a simple problem, the validity of this approach is studied. Then the analysis of the Rama IX Bridge is carried out by this approach, and the numerical results are compared with the stress measurements of a full-scale static loading test (FLT). In all the analyses herein, a finite element program, MARC (1994), is used.

2. Hybrid modeling

2.1 Simply supported thin-walled steel box girder

A simply supported thin-walled steel box girder under a concentrated load at mid span shown in Fig. 1 is analysed by the hybrid modeling. As illustrated in Fig. 2, the central part is modeled by shell elements and the remaining part is by beam elements so as to evaluate the stress at the mid-span section. The former part is called S-Zone and the latter is B-Zone hereafter. Employed in the present study are 4-node shell elements and 2-node beam elements. A rigid plate is attached to the end of S-zone so as to impose the continuity between S-Zone and B-Zone.

Seven different models in terms of L_s/L ($= 0.13750, 0.15625, 0.17500, 0.19375, 0.21250, 0.23125, 1.0$) are constructed and analyses are carried out. The six models are named Model I to VI in the order of increasing L_s/L , and the model of $L_s/L = 1.0$ is called the shell-element model. Due to symmetry, only a quarter needs to be modeled.

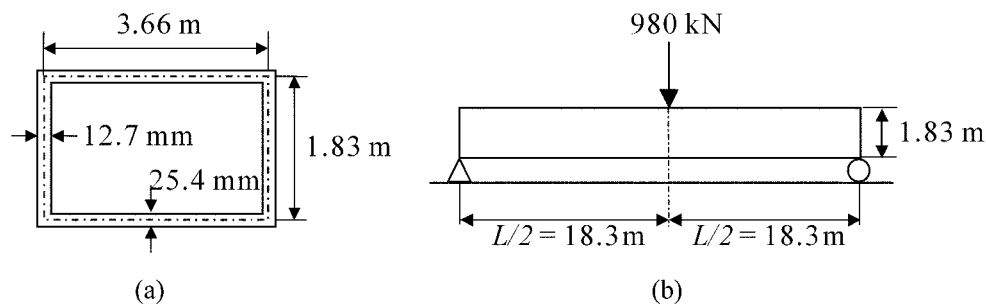


Fig. 1 A simply-supported steel box girder: (a) Cross section, (b) Loading condition

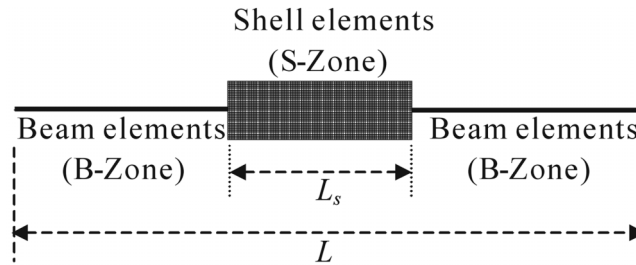


Fig. 2 Hybrid modeling of a box girder

2.2 Numerical results

The distributions of the normal stress in the longitudinal direction, σ_L , across the upper flange width of the box girder at mid-span section are shown in Fig. 3. As L_s/L becomes larger, σ_L tends to converge to that given by the shell-element model. The numerical values of σ_L at the corner and the mid-width of the upper flange are presented in Table 1 together with the percentage differences from that of the shell-element model.

Table 1 indicates that the percentage difference from the result of the shell-element model becomes less than 1% when L_s/L is 0.2125 or bigger. The table also shows the value of $L_s/2b$ where b is the width of the cross section, i.e., 3.66 m. It is then realized that the percentage difference becomes less than 1% when $L_s/2b$ exceeds 1.0. Since $L_s/2$ represents the distance from the point of interest, i.e., the mid-span, to the end of S-Zone, the result herein implies that the influence of the modeling by beam elements, i.e., B-Zone, becomes insignificant when the distance between the point of interest and the end of S-Zone is bigger than the representative size of the boundary, i.e., b . The number of total degrees-of-freedom of Model V is 49,221, while the shell-element model has 186,531 degrees-of-freedom. Since Model V can yield satisfactory results in practice, the efficiency of the hybrid modeling is thus evident from the computational point of view.

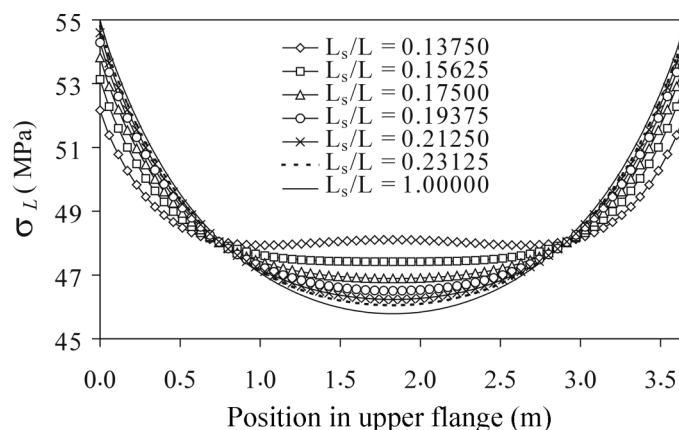


Fig. 3 Effect of L_s on σ_L in an upper flange at mid-span

Table 1 σ_L in a simply supported box girder

Hybrid model	L_s/L	$L_s/2b$	Number of total degrees-of-freedom	Corner	Mid-width of upper flange
				σ_L (MPa)	σ_L (MPa)
I	0.13750	0.68750	35,577	-52.2 (-5.14)	-48.1 (5.05)
II	0.15625	0.78125	38,991	-53.1 (-3.39)	-47.4 (3.56)
III	0.17500	0.87500	42,399	-53.8 (-2.14)	-46.9 (2.40)
IV	0.19375	0.96875	45,813	-54.3 (-1.28)	-46.5 (1.56)
V	0.21250	1.06250	49,221	-54.6 (-0.73)	-46.2 (0.99)
VI	0.23125	1.15625	52,635	-54.8 (-0.37)	-46.1 (0.58)
Shell-element model	1.000	5.000	186,531	-55.0	-45.8

(): Discrepancy from the result of the shell-element model (%)

2.3 Different types of box girder

For further verification of our proposal for the size of S-Zone, $L_s \geq 2b$, the girders with different boundary conditions, loading conditions and proportions are investigated. Fig. 4 illustrates the boundary conditions (simple support and propped cantilever) and loading conditions (concentrated and distributed loads). In addition, various girder proportions are considered: the ratio between the width of cross section to span length $b/L = 0.025, 0.05, 0.1, 0.15$ and 0.2 . The normal stress σ_L at the corner and the mid-width of the upper flange are obtained by analyzing the hybrid models of

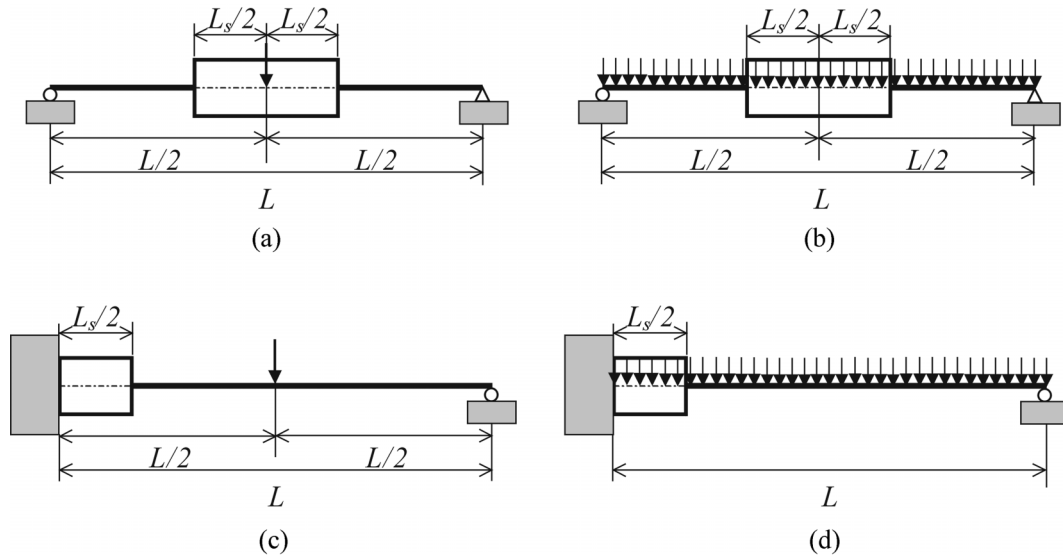


Fig. 4 Hybrid models with different boundary conditions and loading conditions: (a) Simply supported/concentrated load, (b) Simply supported/distributed load, (c) Propped cantilevered/concentrated load, (d) Propped cantilevered/distributed load

Table 2 Discrepancy of σ_L for various girders in Fig. 4

(a) Concentrated load

b/L	Discrepancy from the result of the shell-element model (%)			
	Simply supported girder		Propped cantilevered girder	
	Mid-span section		Fixed end section	
	Corner	Mid-width of upper flange	Corner	Mid-width of upper flange
0.025	-1.46	1.43	-0.49	1.55
0.05	-1.35	1.50	-0.10	1.87
0.1	-1.19	1.58	0.71	2.69
0.15	-1.07	1.65	0.51	3.19
0.2	-0.95	1.72	0.31	2.47

(b) Distributed load

b/L	Discrepancy from the result of the shell-element model (%)			
	Simply supported girder		Propped cantilevered girder	
	Mid-span section		Fixed end section	
	Corner	Mid-width of upper flange	Corner	Mid-width of upper flange
0.025	-1.55	1.39	-0.45	1.56
0.05	-1.50	1.44	-0.07	1.85
0.1	-1.43	1.48	0.49	2.45
0.15	-1.35	1.50	-0.25	2.22
0.2	-1.25	1.54	-1.11	0.08

various girders. The size of S-Zone L_s in those hybrid models is determined by using the criterion $L_s/2b = 1$. Note that $L_s/2$ represents the distance from the point of end of S-Zone to point of interest, i.e., the mid-span for the simply supported girder, the fixed end for the cantilevered and propped cantilevered girders as shown in Fig. 4. The percentage discrepancies of σ_L from the shell-element model are shown in Table 2. It is found that hybrid models give satisfactory results compared to those computed from shell-element models. In particular, the absolute values of percentage discrepancy are in the range of 0.08 to 3.19, and the mean square of percentage discrepancy is equal to 1.5%. Therefore, the hybrid model with $L_s \geq 2b$ yields reasonably accurate results compared to the shell-element model.

3. Local stress analysis of the Rama IX Bridge

3.1 Bridge description

The Rama IX Bridge is a long-span steel cable-stayed bridge with a length of 782 m. It links the eastern (Bangkok) and western (Thonburi) sides of Greater Bangkok, Thailand, by crossing the

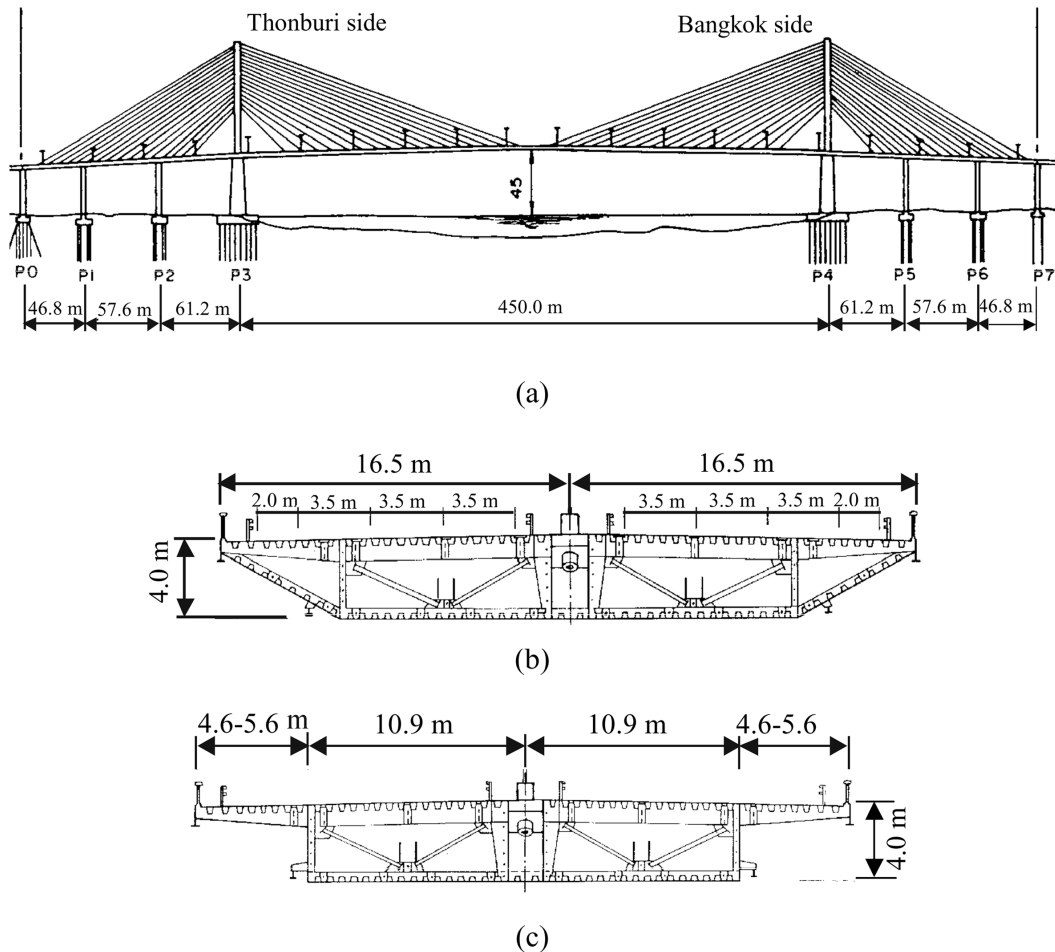


Fig. 5 The Rama IX Bridge: (a) Elevation, (b) Cross section in main span, (c) Cross section in side span

Chao Phraya River and serves to heavy traffic by providing six lanes. This bridge has become an architectural landmark in Bangkok and is considered as a great feat of engineering design and construction technology.

The main structure of the Rama IX Bridge is a single plane symmetric cable-stayed bridge consisting of a clear center span of 450 m and two side spans of 166 m supported on anchor piers as shown in Fig. 5(a). The three spans are supported by the locked coil stay cables, which are anchored in two steel pylons at the ends of the main span and within the steel box girder deck. There are 17 cables radiating in each direction from each pylon: 68 cables in total support the entire deck.

The main cross section of the bridge deck is a three-cell thin-walled steel box girder (Fig. 5 (b)). In the side spans, the bridge deck has cantilevered deck panels of varying width (Fig. 5(c)): the deck width is 31 m at either end of the bridge and 33 m at the pylons. In the center span, the additional triangular cells replace the cantilevered panels so as to reduce aerodynamic loads while increasing torsional rigidity.

The 87-meter high steel pylons pass through the bridge deck, and they are supported on the tops of the concrete piers. The steel pylons are closed rectangular boxes with additional internal framing to carry the cable anchorages.

3.2 Modeling

In FLT, the normal stresses were measured at several locations of the box girder. Since the measured stresses in the transverse diagonal struts are much higher than those at the other locations, only the stresses in the transverse diagonal struts are considered in the present study. Then, the hybrid models of the bridge are constructed so as to evaluate the local stress in the diagonal strut at mid-span (S1) and quarter-span (S2) of the main-span girder. As indicated in Fig. 6, the strut associated with S1 is located at the mid-span and that with S2 is 107 m away from S1. Photo 1 shows those struts.

The Rama IX Bridge is therefore modeled to evaluate the stresses at S1 and S2. Since the hybrid modeling approach is employed, two models of Bridge Models 1 and 2 are constructed for computing the stresses at S1 and S2, respectively: part of a girder around either S1 or S2 is to be S-Zone in those bridge models.

The bridge models herein embody the superstructure of the bridge and accurately represent the geometries of its components such as pylons, cables and a girder. Fig. 7 shows the overview of Bridge Model 1. The details of the modeling for each component are as follows:

1. Two steel pylons are modeled by 2-node beam elements. Axial, bending and shear deformations

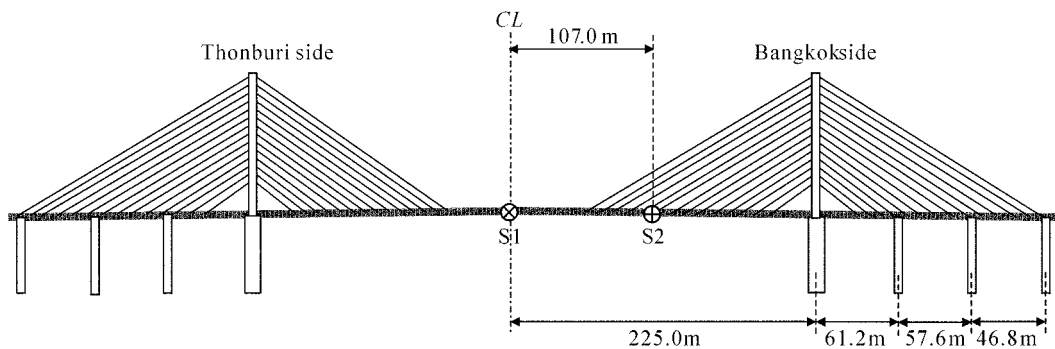


Fig. 6 Locations of S1 and S2

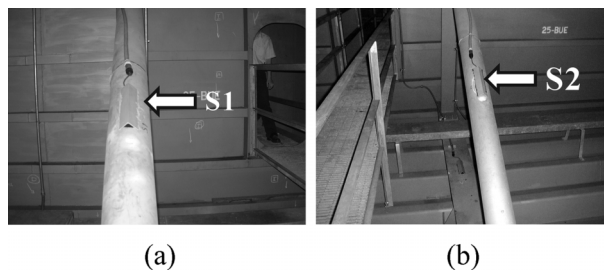


Photo 1 Struts of stress measurements: (a) S1, (b) S2

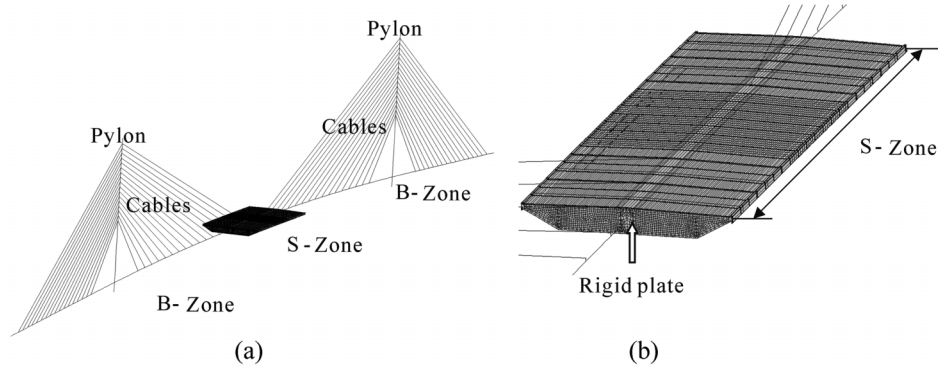


Fig. 7 Bridge Model 1: (a) Overview, (b) Close-up around S-Zone

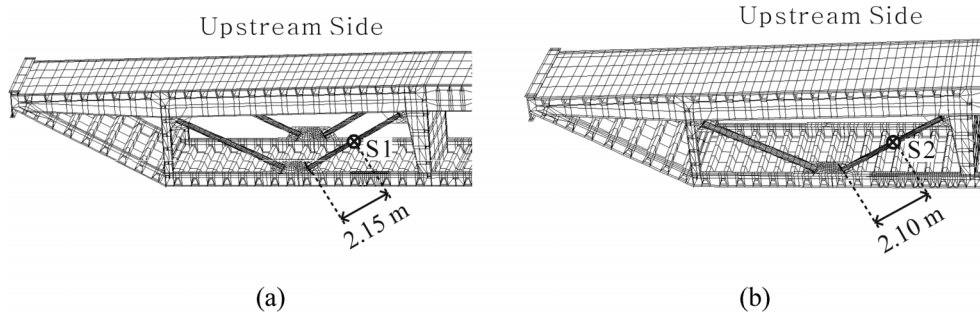


Fig. 8 Close-up of part of S-Zone: (a) Bridge Model 1, (b) Bridge Model 2

are accounted for by the Timoshenko beam theory, and St. Venant's theory is employed for describing torsional behavior.

2. Applying the hybrid modeling, the model of a girder consists of S-Zone and B-Zone. In S-Zone, 4-node shell elements with transverse shear deformation are used to represent the exact geometry of the multi-cellular cross section. All major structural components are modeled as they are, which includes top and bottom decks, stiffening ribs, vertical webs, inclined webs, cross frames and transverse diagonal struts. Fig. 8 presents the details of part of S-Zone for each of Bridge Models 1 and 2. For B-Zone, 2-node beam elements, which are based on the Timoshenko beam theory to account for axial, bending and shear deformations are employed. For the torsional behavior, the multi-cell theory of thin-walled cross section is applied.
3. Cables are modeled by 2-node beam elements representing actual bending stiffness (Gimsing 1997). Axial and bending deformations are evaluated by the elementary beam theory. Torsional and shear distortions are neglected. To take into account the nonlinearity due to the sag of cable stays, the Young's modulus E of the cable is replaced by the cable equivalent modulus of elasticity (Ernst 1965), which is given by

$$E_{eq} = \frac{E}{1 + \frac{AE(wL)^2}{12T^3}} \quad (1)$$



Photo 2 A train of trucks on the outmost traffic lane of the bridge (upstream side)

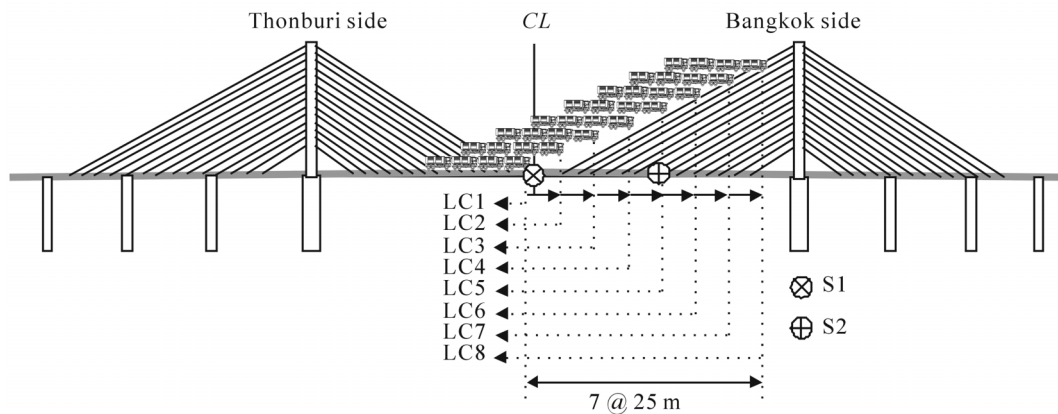


Fig. 9 Schematic of loading cases

where E_{eq} = equivalent cable modulus of elasticity, A = cross sectional area, w = cable weight per unit length, L = horizontal projected length of the cable and T = tensile force in the cable.

The boundary conditions are modeled according to the as-built drawing of the bridge. To sustain the stability, the two steel pylons are linked to the main concrete piers rigidly and neither translate nor rotate at these joints. The girder is rigidly connected to the pylons as well in order to ensure the synchronous movement between the pylons and the girder. On the side span piers, the girder is supported by rocker bearings, which are longitudinally movable hinges, allowing the girder to move in the longitudinal direction and rotate about the transverse axis.

In FLT, a train of four trucks is placed on the outmost traffic lane (upstream side), as shown in Photo 2. Each truck has 10 wheels and its gross weight is known to be 206 kN. Eight different positions of the train are selected, thus conducting eight static loading tests of Loading Cases 1-8 (LC1-LC8). As illustrated in Fig. 9, the static loading test starts with LC1 and the trucks are moved toward the Bangkok side after the completion of each loading test. The distance between the truck position of the two adjacent loading causes such as LC1 and LC2 is 25 m.

The 3D FEA is conducted for local stress evaluation at S1 and S2 under these eight loading conditions of LC1-LC8.

3.3 Numerical results

Fig. 10 shows the hybrid modeling used in the present study. The size of S-Zone represented by L_s is set equal to $L_s/L_m = 0.148$ ($L_s/2b = 1.01$) and to $L_s/L_m = 0.157$ ($L_s/2b = 1.07$) for Bridge Models 1 and 2, respectively, in which L_m is the bridge main span, i.e., 450 m, and b is the maximum dimension of the cross section at the end of S-Zone, i.e., 33 m. This size of L_s is determined based on the previous study of various simple beams that the result can be expected sufficiently close to that of the shell-element model when the value of $L_s/2b$ exceeds 1.0.

For each loading case, the normal stress at S1, σ_{LS1} , and the normal stress at S2, σ_{LS2} , are computed and presented in Fig. 11. This figure also shows the stress measured in FLT. The two

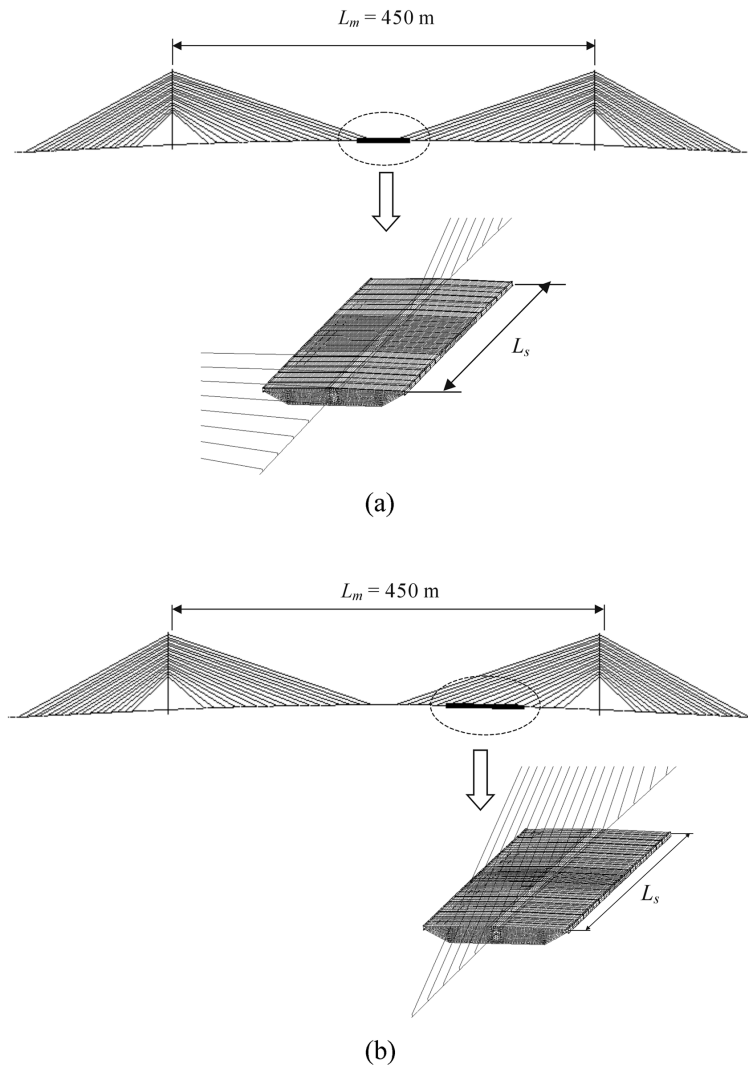


Fig. 10 Hybrid modelings: (a) Bridge Model 1, (b) Bridge Model 2

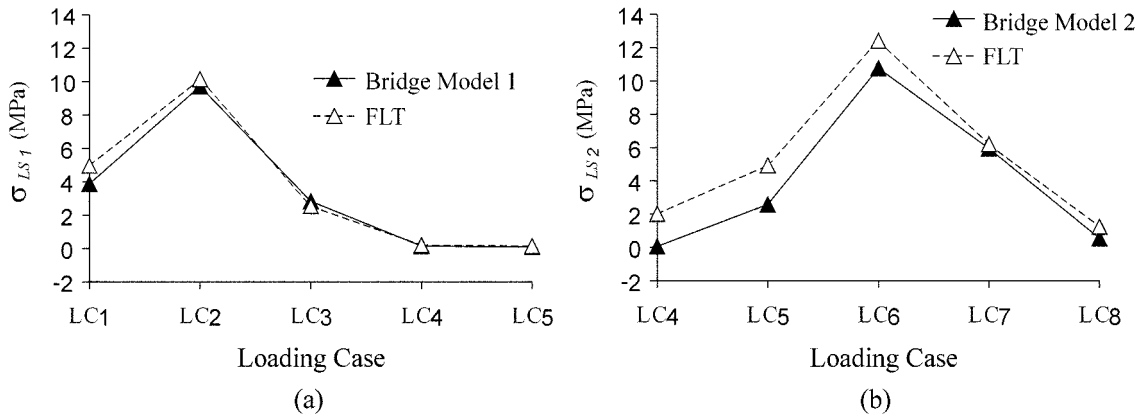


Fig. 11 Normal stresses in the struts: (a) At S1, (b) At S2

stresses of σ_{LS1} are in excellent agreement while some discrepancy is observed in the case of σ_{LS2} . Since much more cables are connected to the girder near S2, the stress state is much more complicated around S2 than S1. This is probably the cause for larger discrepancy in σ_{LS2} . Nevertheless, considering the dimensions and complexity of the Rama IX Bridge, this magnitude of discrepancy in σ_{LS2} may be acceptable in practice.

The numerical results herein imply that there is a good chance to establish an influence line of stress without conducting FLT that is inevitably very expensive and difficult to conduct under heavy traffic condition. The present numerical approach may therefore open a cheaper way of carrying out BWIM (Bridge Weight-In-Motion) that is crucial for making an effective plan for maintenance (Moses 1979).

4. Conclusions

The paper presents the hybrid modeling for the local stress analysis of a long-span cable-stayed bridge. Only part of a bridge in which the point of interest is located is discretized by shell elements while the remaining part is modeled by beam elements. The former is called S-Zone and the latter is B-Zone. A parametric study with respect to the size of S-Zone, i.e., L_s , is conducted for a simply supported box girder. In addition, the extensive numerical investigation using hybrid models with $L_s/2b = 1$ is conducted for different boundary conditions, loading conditions and girder proportions. It is then found that when the ratio of $L_s/2b \geq 1$, the normal stresses computed from hybrid models agree very well with those from shell-element models, and the difference from the shell-element models is sufficiently small. Note that b in $L_s/2b$ is the maximum characteristic length of the cross section at the end of S-Zone. This technique is then applied to the local stress evaluation in the Rama IX Bridge. The numerical results compare very well with the FLT results.

Since FEA with the proposed hybrid modeling technique can reduce computational cost considerably, the present research offers a practical technique for the accurate finite element stress analysis of a long-span cable-stayed bridge, without which such stress analysis would remain in the phase of academic research interest.

Acknowledgements

The present research was partially supported by the Thailand Research Fund through the Royal Golden Jubilee Ph.D. Program (Grant No. PHD/0055/2543) and by the Ministry of Education, Science, Sports and Culture of Japan through Grant-in-Aid for Scientific Research (A) (No. 13355020). It is the outgrowth of the academic agreement between Sirindhorn International Institute of Technology, Thammasat University and Faculty of Engineering, Kyushu Institute of Technology, and has been partially supported also by the two academic bodies. These supports are gratefully acknowledged. Special thanks are given to the Expressway and Rapid Transit Authority of Thailand for providing information on the Rama IX cable-stayed Bridge.

References

- Agrawal, T.P. (1997), "Cable-stayed bridges-parametric study", *J. Bridge Eng.*, **2**(2), 61-67.
- Ali, H.M. and Abdel-Ghaffar, A.M. (1995), "Modeling the nonlinear seismic behavior of cable-stayed bridges with passive control bearings", *Comput. Struct.*, **54**(3), 461-492.
- Au, F.T.K., Cheng, Y.K. and Zheng, D.Y. (2001), "On the determination of natural frequencies and mode shapes of cable-stayed bridges", *Appl. Math. Modeling.*, **25**, 1099-1115.
- Chang, C.C., Chang, T.Y.P. and Zhang, Q.W. (2001), "Ambient vibration of long-span cable-stayed bridge", *J. Bridge Eng.*, **6**(1), 46-53.
- Ernst, H.J. (1965), "Der E-Modul von Seilen Unter Berueck-Sichtigung des Durchhanges", *Der Bauingenieur*, **40**(2), 52-55.
- Gimsing, N.J. (1997), *Cable Supported Bridges*, 2nd ed., John Wiley & Sons, Chichester, England.
- Karoumi, R. (1999), "Some modeling aspects in the nonlinear finite element analysis of cable supported bridges", *Comput. Struct.*, **71**, 397-412.
- Kim, K.S. and Lee, H.S. (2001), "Analysis of target configurations under dead loads for cable-supported bridges", *Comput. Struct.*, **79**, 2681-2692.
- MARC Analysis Research Corporation. (1994), *MARC Manuals-Vol. A-D, Rev. K.6*, Palo Alto, Calif.
- Moses, F. (1979), "Weigh-in-motion system using instrumented bridges", *Transp. Eng. J.*, **105**(TE3), 233-249.
- Shu, H.S. and Wang, Y.C. (2001), "Stability analysis of box-girder cable-stayed bridges", *J. Bridge Eng.*, **6**(1), 63-68.
- Wang, P.H., Lin, H.T. and Tang, T.Y. (2002), "Study on nonlinear analysis of a highly redundant cable-stayed bridge", *Comput. Struct.*, **80**, 165-182.
- Wang, P.H. and Yang, C.G. (1996), "Parametric studies on cable-stayed bridges", *Comput. Struct.*, **60**(2), 243-260.
- Xu, Y.L., Ko, J.M. and Zhang, W.S. (1997), "Vibration studies of Tsing Ma Suspension. Bridge", *J. Bridge Eng.*, **2**(4) 149-156.
- Zhang, Q.W., Chang, T.Y.P. and Chang, C.C. (2001), "Finite-element model updating for Kap Shui Mun Cable-stayed Bridge", *J. Bridge Eng.*, **6**(4), 285-293.